[CANCER RESEARCH 63, 1806–1813, April 15, 2003]

Population Pharmacokinetics of the Photodynamic Therapy Agent 2-[1-Hexyloxyethyl]-2-devinyl Pyropheophorbide-a in Cancer Patients[1]

David A. Bellnier,[2,3] William R. Greco,[2] Gregory M. Loewen, Hector Nava, Allan R. Oseroff, Ravindra K. Pandey, Takaaki Tsuchida, and Thomas J. Dougherty

PDT Center [D. A. B., R. K. P., T. J. D.] and Departments of Cancer Prevention [W. R. G.], Medicine [G. M. L.], Surgery [H. N.], and Dermatology [A. R. O.], Roswell Park Cancer Institute, Buffalo, New York 14263 and Department of Surgery, Tokyo Medical University, Tokyo, Japan [T. T.]

ABSTRACT

Photodynamic therapy is an effective and often curative treatment for certain solid tumors. The porphyrin-based photosensitizer Photofrin, the only Food and Drug Administration-approved drug for this therapy, suffers from certain disadvantages: its complex chemical nature; retention by skin (leading to protracted cutaneous photosensitivity); and less than optimal photophysical properties. In this study, we examine the population pharmacokinetics and cutaneous phototoxicity of 2-[1-hexyloxyethyl]-2-devinyl pyropheophorbide-a (HPPH), a chlorin-type photosensitizer with more favorable photophysical properties. HPPH plasma concentration-time data were obtained in 25 patients enrolled in Phase I-II clinical trials for the treatment of partially obstructive esophageal carcinoma, high-grade dysplasia associated with Barrett's esophagus, carcinoma of the lung, or multiple basal cell carcinomas. Doses of 3, 4, 5, or 6 mg/m^2 were administered as 1-h i.v. infusions. The pharmacokinetic data for each patient were fitted with a standard two-compartment (biexponential) model with continuous infusion. The model fitting approach was iteratively reweighted nonlinear regression, with weights equal to the reciprocal of the square of the predicted HPPH plasma concentrations. The complete set of data for all 25 patients was then fitted simultaneously with nonlinear mixed effects modeling. Cutaneous phototoxicity responses were determined, as a function of time after HPPH infusion, following exposure to various doses of light from a solar simulator. The estimates of the population mean (variance) for each parameter were as follows: volume of distribution (V_C), 2.40 liters/m^2 (0.259); steady-state volume (V_{SS}), 9.58 liters/m^2 (11.6); systemic clearance (CL), 0.0296 liter/h/m^2 (0.000094); and distributional clearance (CL_D), 0.144 liter/h/m^2 (0.00166). These parameters were independent of dose. Clearance increased with age. A relative error model was used for the difference in the raw and fitted data, and the overall coefficient of variation estimate across all of the data was 14.5%. The estimated mean population α and β half-lives (95% confidence interval) were 7.77 h (3.46–17.6 h) and 596 h (120–2951 h), respectively. High-performance liquid chromatography analysis of serum showed no circulating HPPH metabolites, and *in vitro* incubation of HPPH with human liver microsomal preparations resulted in no metabolite or glucuronic acid-HPPH conjugate production. A minimal skin response to the solar simulator was observed, mostly in patients treated with the highest dose of HPPH, 6 mg/m^2. All of the HPPH pharmacokinetic parameters were consistent with a highly lipophilic agent that is concentrated in plasma and is nearly 100% bound to plasma proteins; this was verified by plasma protein binding studies. Whereas low concentrations of HPPH can be detected in plasma several months after a single infusion, no instances of cutaneous photosensitivity have been noted in these patients. In general, HPPH pharmacokinetic profiles are readily predictable from the global population model. This is the first comprehensive human population pharmacokinetic/pharmacodynamic study of a clinical anticancer photodynamic therapy agent.

INTRODUCTION

PDT[4] has been successful in the management of a wide variety of solid, malignant tumors (1). PDT is based on the ability of certain drugs to localize in tumors and generate cytotoxic reactive oxygen species, particularly singlet oxygen, upon illumination with visible light (2). Only porfimer sodium (Photofrin), a complex mixture of porphyrin derivatives, has been approved for this use in the United States, Canada, Europe, and Japan (1). Unfortunately, Photofrin absorbs light only weakly at the longest possible wavelength (λ_{max} = 630 nm; molar extinction coefficient $\epsilon_{630} \sim 2000$ M^{-1} cm^{-1}), and light of this wavelength penetrates tissue suboptimally (3). In addition, use of this photosensitizer is associated with prolonged but diminishing skin photosensitivity lasting a month or more after injection (4). As a result, a number of other drugs with more optimal photophysical properties (*e.g.*, longer wavelength absorption and greater molar extinction coefficients) and shorter durations of skin photosensitivity are being examined as photosensitizing agents (5).

One such drug is HPPH (Photochlor), a chlorin-based molecule (6) (Fig. 1, *inset*). HPPH is an extremely hydrophobic compound that was found, in a quantitative structure-activity relationship study that addressed the general property of lipophilicity (7), to be the most effective photosensitizer against murine tumors amongst a series of homologues with different numbers of methylene groups on the ether function. This compound strongly absorbs light ($\epsilon_{665} \sim 47{,}000$ M^{-1} cm^{-1}) at 665 nm, so that penetration into tumor tissue is increased *vis-à-vis* Photofrin (3).

We are currently investigating HPPH in a number of dose-ranging studies in cancer patients. The clinical program consists of four Phase I-II drug-dose-ranging and light-dose-ranging studies in patients with basal cell carcinoma(s), obstructive esophageal cancer, Barrett's esophagus with high-grade dysplasia, or early- or late-stage lung cancer. Patients enrolled in these studies undergo cutaneous photosensitivity testing using a commercial solar simulator, if practicable. Preclinical pharmacokinetics of HPPH in dogs (8) and tissue distribution data in mice given ^{14}C-radiolabeled HPPH (9) have been reported, but no prior publication has examined HPPH pharmacokinetics in patients. Therefore, an analysis of pooled pharmacokinetic data from 25 patients undergoing PDT using this drug is reported. We also provide cutaneous phototoxicity data and analysis and briefly discuss the clinical responses of these patients to HPPH PDT.

MATERIALS AND METHODS

Clinical Studies. Pharmacokinetic data were obtained from 9 patients from the esophageal carcinoma study, 11 patients from the Barrett's esophagus/dysplasia study, 3 patients from the basal cell carcinoma study, and 2 patients from the lung carcinoma study. Informed consent was similar for all the studies and followed prescribed NIH guidelines. All studies were approved by the institute review board and the Food and Drug Administration. Median (range) baseline characteristics of the patients were as follows: age, 70 years (37–89

Received 9/13/02; accepted 2/19/03.

The costs of publication of this article were defrayed in part by the payment of page charges. This article must therefore be hereby marked *advertisement* in accordance with 18 U.S.C. Section 1734 solely to indicate this fact.

[1] Supported in part by NIH Grant P01 CA55791. This work utilized core facilities supported in part by Roswell Park Cancer Institute's National Cancer Institute-funded Cancer Center Support Grant CA16056.

[2] These authors contributed equally to this work.

[3] To whom requests for reprints should be addressed, at PDT Center, Roswell Park Cancer Institute, Elm and Carlton Streets, Buffalo, NY 14263.

[4] The abbreviations used are: PDT, photodynamic therapy; HPPH, 2-[1-hexyloxyethyl]-2-devinyl pyropheophorbide-a; HPLC, high-performance liquid chromatography; BSA, body surface area.

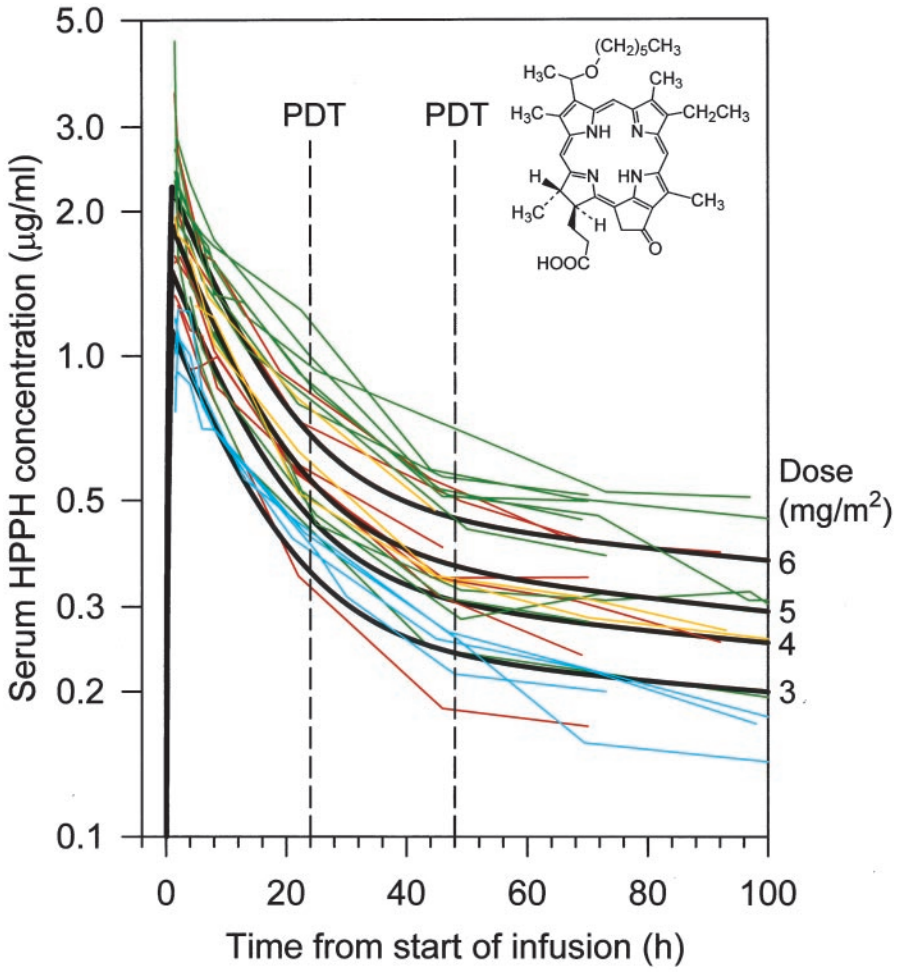

Fig. 1. The time course of human HPPH pharmacokinetics. The *colored line plots* represent the raw data (one plot/patient), with the *sharp bends* in the plots representing data points. The 4 *blue plots* represent patients who received 3 mg/m^2 HPPH; 7 *red plots* represent patients who received 4 mg/m^2, 3 *yellow plots* represent patients who received 5 mg/m^2; and 11 *green plots* represent patients who received 6 mg/m^2. The set of *thicker smooth black curves* is the final best fit of the global model to the complete data set for the four doses labeled to the *right* of the figure. The *vertical dashed lines* represent the two times that light is routinely administered for photodynamic therapy with HPPH. *Inset*, the structure of HPPH.

years); weight, 75.1 kg (47.0–123 kg); and body surface area, 1.94 m^2 (1.42–2.44 m^2). Of the 25 patients, 21 were male, and 4 were female.

HPPH was manufactured at the University of California Davis under good manufacturing practice conditions by one of us (R. K. P.). Preparation and characterization of HPPH were as described previously (9); the injectable drug was formulated in 5% dextrose in sterile water containing 2% ethanol and 1% polyoxyethylene sorbitan monooleate (Tween 80) and kept frozen before use. Doses were administered i.v. over 1 h at an infusion rate of 110 ml/h. Pharmacokinetic data were available for doses of 3 mg/m^2 (n = 4), 4 mg/m^2 (n = 7), 5 mg/m^2 (n = 3), and 6 mg/m^2 (n = 11). Blood samples were collected in anticoagulant-free tubes on 4–13 occasions/patient between the end of infusion and study day 143. A total of 193 blood samples were obtained after HPPH infusion; in some cases, preinfusion blood samples were acquired to establish baseline serum fluorescence levels (see below).

Blood Sampling and Photosensitizer Analysis. HPPH serum levels were monitored using a fluorescence assay because of the high quantum fluorescence yield of the drug ($\Phi_F \sim 0.45$) and the inherent increased sensitivity of spectrofluorimetry over absorption-based methods (*e.g.*, spectrophotometry, HPLC). Serum was isolated by centrifugation, and samples were kept at −70°C until assayed. Serum concentrations of HPPH were determined by admixture with Solvable (Packard Bioscience, Meriden, CT) and heating at 53°C followed by analysis of fluorescence emission spectra as described previously (10). Briefly, after treatment with Solvable and heat, each sample was placed in a quartz cuvet, and a fluorescence emission spectrum (λ_{ex} = 412 nm) was obtained using a commercial fluorimeter (model FP-777; JASCO, Inc., Easton, MD). Typically, 3 replicates/time point/patient were analyzed. The amplitude of the fluorescence emission maximum (λ_{em} = 670 nm), following baseline correction, was compared with a standard curve obtained by processing known amounts of HPPH in Solvable-containing serum from volunteers. No patient sera obtained before infusion had measurable fluorescence corresponding to the HPPH fluorescence spectrum.

Studies of the Binding of HPPH to Plasma Proteins. The binding of HPPH to protein and lipoprotein components in human plasma was assessed using KBr density gradient analysis. This system was a modification of the previously published procedure of Woodburn and Kessel (11). Briefly, blood was collected from a donor using EDTA as the anticoagulant to minimize lipoprotein oxidation. Erythrocytes were removed by centrifugation, and the plasma was incubated with HPPH at a concentration of 10 μM. After 24 h at 4°C, the plasma was mixed with 0.15 M NaCl and brought to a density of 1.21 g/ml with solid KBr. A portion of the resulting mixture was layered over a KBr solution (density, 1.27 g/ml) in polyallomer centrifuge tubes (Beckman Instruments Inc., Palo Alto, CA). The tubes were filled with isotonic saline and spun in a Beckman TL-100 tabletop ultracentrifuge for 1 h. The tubes were fractionated from the top; a total of 25 fractions were collected. Each fraction was diluted with 1% polyoxyethylene sorbitan monooleate (Tween 80), and the relative concentration of HPPH was assessed by fluorescence.

HPPH Metabolism Studies. A study was carried out to identify circulating metabolites of HPPH. For this, serum was isolated, by centrifugation, from blood drawn from patients at various times (1, 7, 24, 48, and 96 h) after the end of the HPPH infusion. The serum was vortex-mixed with methanol in microcentrifuge tubes. Two to four serum samples from different patients were analyzed for each time point. This mixture was then centrifuged at 10°C to pellet the precipitated protein. The supernatant was removed and analyzed by HPLC. Sera isolated from patients who had not yet been injected with photosensitizer were used as controls.

To study whether HPPH could be metabolized by liver enzymes *in vitro*, the drug was incubated with mixed sex, pooled human liver microsomes according to the provided protocol (In Vitro Technologies, Baltimore, MD); the cryopreserved microsomes had been characterized previously by the supplier for a wide variety of isozyme activities. Briefly, solid HPPH was dissolved in acetonitrile and mixed with potassium phosphate buffer (pH 7.4) and the pooled microsomes, followed by warming. After 5 min, warm NADPH regen-

erating system was added to the reaction mixture. After shaking at 37°C for 1 h, the reaction was terminated with an equal volume of acetonitrile. The tubes were centrifuged to pellet the precipitated protein, after which the supernatant was removed and analyzed by HPLC.

To study type II conjugation of HPPH, the protocol was modified by the addition of uridine-5′-diphosphoglucuronic acid and 3′-phosphoadenosine 5′-phosphosulfate to the NADPH regenerating system. Samples were shaken in the heated water bath and centrifuged to precipitate protein, as described above. The supernatants were analyzed by HPLC.

Reverse-phase HPLC was used for identification of HPPH and its metabolites and conjugates. Separation was carried out on an RP-8 LiChrospher 100 column (Merk KGaA, Darmstadt, Germany) using mobile phases consisting of 60% methanol in 10 mM sodium phosphate buffer and 90% methanol in 2 mM sodium phosphate buffer, both pH 7.5. The sample was monitored by absorption measurements at 405, 450, and 665 nm with a diode array UV/VIS detector (Hewlett Packard 1100 Series; Agilent Technologies, Palo Alto, CA).

Solar Simulator Studies. The magnitude and duration of cutaneous photosensitivity in patients who were given HPPH were determined. For this, the skin of the medial forearm was exposed to a simulated solar spectrum (350–2500 nm) produced by a 300 W solar simulator (model 81250 with an AM1.5 direct filter; Oriel Corporation, Stratford, CT). For each test, four 1.0-cm^2 spots were exposed to light for 10, 15, 20, or 30 min at a fluence rate of 74 mW/cm^2. Skin responses were graded approximately 24 h after exposure. Baseline reactions were obtained by exposing the forearm skin to the solar simulator light before HPPH was injected, typically on the same day. After receiving injection, each patient was then tested daily for 3 days and occasionally upon return for clinical follow-up. The scale for grading skin photosensitivity can be found in the legend to Table 2.

Pharmacokinetic Modeling. The HPPH plasma concentration with time data for each patient were fit with a two-compartment (biexponential) model with continuous infusion (Eq. 1; note that all equations are listed in the "Appendix"). Eq. 1 was adapted from the standard equation for a two-compartment model with immediate bolus injection (12) by the method of Loo and Riegelman (13) to account for the effect of the 1-h infusion. The model fitting approach was iteratively reweighted nonlinear regression, with weights equal to the reciprocal of the square of the predicted HPPH plasma concentrations. This procedure was run with proc NLIN (14) with SAS version 8.12 on an Intel Pentium IV-based microcomputer. From the four estimated parameters, A, B, half-time for first exponential term ($t_{1/2\alpha}$), and half-time for second exponential term ($t_{1/2\beta}$), other pharmacokinetic parameters were calculated (Eqs. 2–7), including rate constant for first exponential term ($\alpha = \ln(2)/t_{1/2\alpha}$), rate constant for second exponential term ($\beta = \ln(2)/t_{1/2\beta}$), area under the concentration-time plasma HPPH curve from time 0 to infinity (AUC), mean residence time (MRT), plasma clearance (CL), distributional clearance (CL_D), volume of distribution of the central compartment (V_C), and volume of distribution at steady state (V_{SS}). The estimated concentration of HPPH in the plasma (C_P) at 24 and at 48 h was calculated from Eq. 1 with the fitted parameters (A, B, $t_{1/2\alpha}$, and $t_{1/2\beta}$) for each patient.

The possible relationships between specific parameters and potential covariates, including age, gender, body surface area (BSA), body weight, total dose of administered HPPH (mg), and dose of HPPH (mg/m^2), were explored by making bivariate scatter plots.

Nonlinear mixed effects modeling was applied to the complete data set of 193 data points from 25 patients simultaneously with proc NLMIXED (15), with the first order (firo) option for integration and the default options for all other choices, with SAS version 8.12 on an Intel Pentium IV-based 2.0 GHz microcomputer. A typical run, such as the final run, which included 10 estimable parameters, took approximately 10 s. In contrast, when using the option for integration recommended by the SAS manual, adaptive Gaussian quadrature, no run with 10 estimable parameters ever finished; runs were stopped at 120 h or less.

The actual model that was fitted to the complete data set included 14 equations from the Appendix (Eqs. 16–19, 8–15, 1, and 20, in that order). Eqs. 16–19 scale and transform the set of four physiological parameters, CL, CL_D, V_C, and V_{SS}, so that they are all in the same order of magnitude. This is important for optimizing the efficiency of the fitting algorithms. Eq. 17 transforms V_{SS} to $\ln(V_{SS})$. This gave the distribution of the parameter more of a Gaussian shape; a normal distribution for each parameter among patients is a common and desirable assumption in nonlinear mixed effects modeling. Eq. 18 expresses the relationship between CL and age; an initial look at the individual patient CL against age hinted at a linear relationship. The inclusion of a covariate in the overall model has the potential to explain some of the variation among patients for that parameter. Eqs. 16–19 include the random parameters b_1, b_2, b_3, and b_4. As is usual, it was assumed that the population mean for each of b_1, b_2, b_3, and b_4 is zero, and estimation was attempted for only the population variances and covariances for the set of four random variables. It was further assumed that each of these random variables was normally distributed.

Eqs. 8–15 map the set of four physiological pharmacokinetic parameters to the set of four empirical pharmacokinetic parameters: A, B, $t_{1/2\alpha}$, and $t_{1/2\beta}$. Eq. 1 includes the set of four empirical parameters and is the structural model fit directly to the data. Combining Eqs. 8–15 with Eq. 1 allows the four physiological pharmacokinetic parameters to be estimated directly and facilitates the inclusion of covariates that affect the physiological parameters.

The error variance model used for this study is Eq. 20. It was assumed that errors were normally distributed with a population mean of zero. Contributions to the total error come from both assay error and model misspecification error. This is a relative error model, and the square root of ϕ_2 is the overall coefficient of variation for the data.

To apply NLMIXED to the raw data, the above equations were coded into the SAS procedure language in the following order: Eqs. 16–19; 8–15; 1; and 20. This final model was built up gradually by adding/subtracting logical model components and covariates. The log ratio test ($P < 0.05$) and the examination of various diagnostic plots were used in the model building process to decide upon the inclusion/exclusion of model components and covariates. The SAS code for the final run of the complete model will be emailed to any interested persons upon request.[5]

RESULTS AND DISCUSSION

Fig. 1, *inset*, shows the structure of HPPH. HPPH is a highly lipophilic drug with a log *P* of ~5.6 at physiologic pH (7), and it is formulated in 2% ethanol and 1% polyoxyethylene sorbitan monooleate (Tween 80). Its large molar extinction coefficient in the red region of the visible spectrum ($\epsilon_{665nm} \sim 47{,}000\ M^{-1}\ cm^{-1}$) and singlet oxygen quantum yield (Φ_Δ) of 0.48 (16) make it an attractive candidate for use in the PDT of malignant tumors.

PDT with HPPH appears to be a relatively effective treatment. In the first Phase I-II clinical study with HPPH, patients with partially obstructive esophageal cancer received a starting dose of 6 mg/m^2 HPPH and a light dose of 150 J/cm ($\lambda = 665$ nm) delivered endoscopically 48 h after injection, based on extensive preclinical pharmacokinetic and toxicological information. This is a palliative treatment meant to relieve difficulty in swallowing. Initially, this low dose, equivalent to approximately 0.15 mg/kg body weight and the lowest of three planned escalating doses, was expected to be ineffective but was required by the Food and Drug Administration based on the data presented to them for obtaining permission to initiate a human clinical trial. However, we found that when examined endoscopically 2 days after PDT, the first and all subsequent patients treated with this dose achieved a brisk response with extensive necrosis of the tumor within the esophagus. Six of eight patients with follow-up experienced palliation of symptoms but no increase in survival as expected (median survival, 8 months); however, one patient with fairly limited disease achieved a complete response for 1.5 years. This result is similar to that for Photofrin-based PDT in such patients.

Three patients with multiple basal cell carcinomas received 3 mg/m^2 HPPH (one-half the dose used for the esophageal patients, above) followed (*a*) 24 h later by 50 or 150 J/cm^2 or (*b*) 48 h later by 150–200 J/cm^2 of 665 nm light. Follow-up of these patients to date indicated that most lesions had complete responses with a drug-light

[5] Available upon request from William R. Greco (william.greco@roswellpark.org).

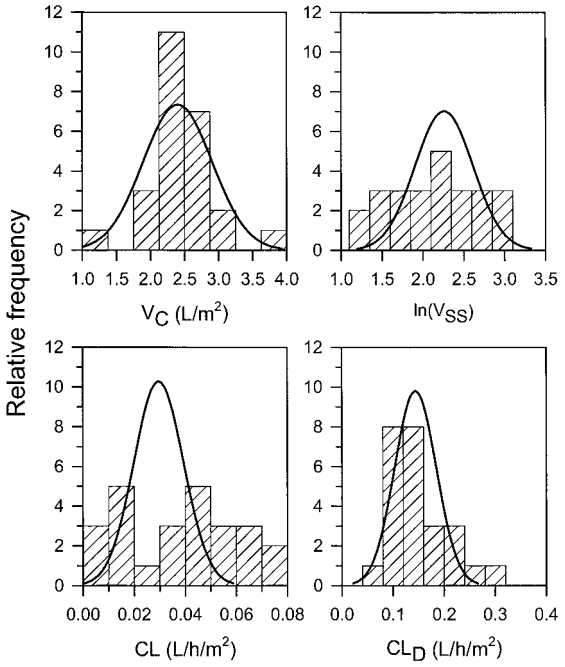

Fig. 2. The distribution of physiological pharmacokinetic parameters among patients. The histograms represent the distribution of the parameters CL, CL_D, V_C, and V_{SS}, which were calculated with Eqs. 2–7, from the set of four empirical pharmacokinetic parameters (A, B, $t_{1/2\alpha}$, and $t_{1/2\beta}$), which were estimated by fitting Eq. 1 to the raw data for each patient individually. The *Gaussian curves* represent the final best fit of the global model to the complete data set.

interval of 24 h and complete and partial responses with an interval of 48 h.

A third Phase I-II trial is the study of PDT of high-grade dysplasia in Barrett's esophagus. Clinical information for these patients is still being accumulated, although it appears that a 3 mg/m^2 HPPH dose is ineffective, whereas higher doses of 4, 5, or 6 mg/m^2 may be capable of destroying both the dysplasia and most of the Barrett's esophagus when treated with 150 J/cm 665 nm light 48 h after injection.

Up to now, three patients have been treated for lung cancer with HPPH (4 mg/m^2), with two complete responses and one recurrence 1 month after treatment. Only 1 patient of 25 patients treated to date has reported a cutaneous reaction to sunlight, which may have been unrelated to the HPPH.

Each set of HPPH pharmacokinetic data, one per patient, was initially fit with both a one-compartment model (data not shown) and a two-compartment model (Eq. 1 in "Appendix"), the four empirical parameters (A, B, $t_{1/2\alpha}$, and $t_{1/2\beta}$) were estimated, and the four physiological parameters (CL, CL_D, V_C, and V_{SS}) were calculated. It was clear from visual inspection that a one-compartment model was inadequate for fitting the data, that a two-compartment model fit very well, and that there were insufficient data to characterize a three-compartment model. Each 25-patient set of the four empirical parameter estimates was plotted against dose of HPPH, patient weight, patient BSA, and patient age. Because V_C was linearly related to BSA (data not shown), it was decided to divide V_C (and the other three physiological parameters) by BSA for further analyses. The sum of A + B was linearly related to dose of HPPH, and this allowed us to assume linear pharmacokinetics for further analyses. None of the four physiological parameters was related to dose of HPPH in any obvious manner.

The results for the population pharmacokinetic analysis of HPPH are shown in Figs. 1–3 and Table 1. In Fig. 1, the final global fitted model is represented by the *thick black curve*, and the raw data are represented by the *thin colored curves* (see legend). Overall, from the perspective of Fig. 1, the final global model fit the raw data extremely well. Note that the assumption that pharmacokinetics are linear in dose is supported from the good fit of the global model to the data in Fig. 1. The predicted mean C_{max} (maximum plasma HPPH concentration achieved at the end of the 1-h infusion) values were 1.13, 1.50, 1.87, and 2.25 μg/ml for doses of 3, 4, 5, and 6 mg/m^2, respectively. The *vertical dashed lines* in the figure represent the two times that light is normally administered for PDT with HPPH. A two-compartment pharmacokinetic population model was shown to be vastly superior to the one-compartment population model via the likelihood ratio test ($P \ll 0.01$); a three-compartment population model could not be successfully fit to the data.

In Fig. 2, the parameter estimates for the fits to the individual patient curves are represented by the normalized histograms, and the final fitted global model is represented by the *thick black Gaussian curves*. Again, the concordance of the individual patient parameters and the global fitted model is excellent. Note that for seven of the patients, adequate HPPH plasma measurements were not observed at later time points to allow neither the accurate estimation of the β phase half-life nor any of the physiological parameters that are highly dependent on this empirical parameter. The population nonlinear mixed effects modeling approach compensates for this experimental design fault, and therefore, its result, the Gaussian curves, is much more credible than the individual patient parameter estimate histograms. This set of four Gaussian curves provides an excellent prediction of the distribution of physiological parameters (*i.e.*, volumes and clearances) for patients given HPPH by i.v. infusion. When normalized by the BSA, all of the physiological parameters, including V_{SS}, were independent of dose of administered HPPH, at least from 3 to 6 mg/m^2. The use of the model building tool (the likelihood ratio test) yielded the unambiguous result that age was a significant covariate for CL but not a significant covariate for CL_D, either with or without the age dependency of CL in the global model.

Table 1 includes the 10 parameter estimates from the final global model, along with a SE for each estimate and a 95% confidence interval. The only population parameters that were not statistically significant ($P > 0.05$) were the population variances for CL and CL_D. The estimated population parameter, V_{SS}, and the estimated population variance for V_{SS}, $s^2(V_{SS})$, along with SEs and 95% confidence intervals, were approximated from the results for ln(V_{SS}) and

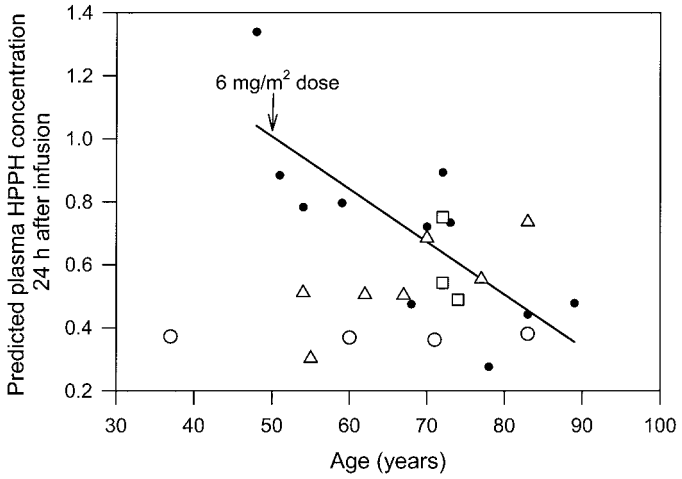

Fig. 3. Relationship of the 24 h postinfusion HPPH plasma concentration predicted from the fit of Eq. 1 to HPPH plasma concentration data from each individual patient to patient age. ●, patients given 6 mg/m^2; □, patients given 5 mg/m^2; △, 4 mg/m^2; the ○, patients given 3 mg/m^2. The *line* was fit with unweighted linear regression to the data from the 11 patients given 6 mg/m^2. The parameter estimates ± SE for this fit were as follows: *y*-intercept = 1.84 ± 0.32; slope = −0.0167 ± 0.0047.

Table 1 *Final parameter estimates*

Parameter	Units	Parameter estimate	SE of parameter estimate	Lower bound of 95% confidence interval	Upper bound of 95% confidence interval
V_C	Liter(s)/m^2	2.40	0.12	2.17	2.63
ln(V_{SS})	Unitless[a]	2.26	0.061	2.13	2.38
V_{SS}[b]	Liter(s)/m^2	9.58	1.1	8.41	10.8
CL	Liter(s)/h/m^2	0.0296[c]	0.0022	0.0342	0.0250
CL_D	Liter(s)/h/m^2	0.144	0.0097	0.124	0.164
$s^2(V_C)$[d]	(Liter(s)/m^2)^2	0.259	0.10	0.0432	0.475
s^2(ln(V_{SS}))	Unitless[a]	0.126	0.054	0.0126	0.239
$s^2(V_{SS})$[b]	(Liter(s)/m^2)^2	11.6	5.0	1.16	21.9
s^2(CL)	(Liter(s)/h/m^2)^2	0.0000940	0.000046	—[e]	0.000189
$s^2(CL_D)$	(Liter(s)/h/m^2)^2	0.00166	0.00084	—[e]	0.00341
cov(V_C*ln(V_{SS}))	Liter(s)/m^2	0.148	0.063	0.0173	0.279
ϕ_2	Unitless	0.0211[f]	0.0033	0.0142	0.0280

[a] Even though V_{SS} has units of liters/m^2, the logarithm of a number must be unitless; there is an implicit multiplication of V_{SS} by a constant equal to 1 (liters/m^2)$^{-1}$ before the logarithmic transformation is applied.

[b] The actual estimated parameter was ln(V_{SS}); V_{SS}, its SE, and 95% confidence interval were calculated by transformation with the exponential function. The estimated population variance of V_{SS}, along with its SE and 95% confidence interval were calculated with the delta formula approximation for the variance of a function of a random variable.

[c] The actual parameter estimated, along with its SE, was 0.000794*(age − 30 years) ± 0.000060*(age − 30 years). The numbers in the table are the mean of the calculated systemic clearances taking into account age for the 25 patients, and the mean of the calculated SEs taking into account age for the 25 patients.

[d] The population variance parameter for each structural parameter is designated as s^2(.).

[e] The lower 95% confidence limits for the population variances of the systemic and distribution clearances were reported by NLIN as being negative; the estimates of the population variances of both clearances just missed statistical significance at the 0.05 level; $P = 0.052, 0.063$, respectively. Thus, the lower 95% confidence limit is greater than zero but unknown.

[f] Because of the structure of the error model, the square root of ϕ_2, 0.145 or 14.5%, can be interpreted as the coefficient of variation of the observed data; *i.e.*, the SD of the differences at each time point for each patient between the raw data and the fitted model, divided by the value of the fitted model.

s^2(ln(V_{SS})). Note that the population parameter, CL, itself, was not estimated directly; rather the linear coefficient of Eq. 18, which relates CL to age, was directly estimated, as is explained in footnote [c] of Table 1. Note that only one population covariance term, that for the covariance between V_C and ln(V_{SS}), was estimated. After many attempts to include more than one population covariance parameter, it became clear that the data from 25 patients had only enough information for one, and the covariance parameter listed in the table was estimated the best. From knowledge of the dose of HPPH and the age of the patient, along with the information in Table 1, one can estimate the mean pharmacokinetic profile for any new patient and can also predict confidence bounds around this mean profile.

The mean population α and β half-lives, calculated from the physiological population parameters in Table 1, were 7.73 and 251 h, respectively. When Eq. 1 was fit directly to the whole 25-patient data set with nonlinear mixed effects modeling, the estimated mean population α and β half-lives (95% confidence interval) were 7.77 h (3.46–17.6 h) and 596 h (120–2951 h), respectively. The discrepancy in the β half-life estimates from the two different approaches for estimation underscores the uncertainty in the population distribution of the β half-life. Both the α and β half-lives are relatively long, as compared with many other drugs; note that the Food and Drug Administration-approved photodynamic sensitizer Photofrin has initial and terminal population half-lives of 16.1 h and 155.6 days (17). Both these drugs leave the plasma very slowly, which may account for their prolonged clinical activity.

The very low clearances and volumes for HPPH listed in Table 1 are consistent with a highly lipophilic agent that is concentrated in the plasma, where it is almost 100% bound to plasma proteins. The binding of HPPH to serum proteins was measured using KBr density gradient ultracentrifugation. The majority of HPPH partitioned to low density lipoprotein (53%), albumin and other heavy proteins (27.5%), and high density lipoprotein (15%), whereas the remaining drug (4.5%) was either associated with very low density lipoprotein or unbound.

The results from the present human HPPH pharmacokinetic study were compared with results from previous pharmacokinetic studies in the mouse (9) and in the dog (8). Conversion factors from Freireich *et al.* (18) were used to calculate volumes and clearances for the mouse, dog, and human in common units. Overall, the concordance of the pharmacokinetic results was very good. For example, the estimated mouse (20 g body weight) total V_C was 1.25 ml, which is very close to the estimated mouse plasma volume of 1.40 ml. The estimated mouse CL was 0.019 liter/h/m^2, which is close to the value of 0.0296 liter/h/m^2 found for the human in the current study. The estimated V_C for the dog (24.6 kg) was 0.069 liter/kg, which is almost exactly equal to the 0.07 liter/kg empirical factor (19) for estimating plasma volume. The CL for the dog was estimated to be 0.102 liter/h/m^2, which is about three times the average CL estimated for the human in the current study. Hence, in three species, HPPH is cleared very slowly from the central plasma compartment, and the V_C is close in size to the estimated plasma volume. Therefore, most of the HPPH in plasma is likely bound to plasma protein.

A possible explanation for the increase in CL with age involves the binding of HPPH to albumin. Because plasma albumin concentration tends to decrease with age (20), older patients may have more unbound plasma HPPH, which would result in a faster clearance (20). Although not labeled in Fig. 1, the HPPH concentration-time curves for the patients given 6 mg/m^2 (the *green lines*) were roughly rank-ordered, with the younger patients having the higher concentrations, and the older patients having the lower concentrations at each time point. This is shown convincingly in Fig. 3.

Table 2 shows the relationship among HPPH dose, individual patient AUC, and 24 h predicted HPPH plasma concentration, and the results of a solar simulator test for 19 of the total 25 patients in this study. The results suggest that increasing the dose of HPPH to 6 mg/m^2 increases the likelihood of postinfusion positive solar simulator tests. However, also note that the most striking solar simulator effects, those for patient 17, were still quite mild, consisting of pronounced erythema, but without tissue edema. In addition, note that the two listed individual pharmacokinetic parameters (individual patient AUC and 24 h predicted HPPH plasma concentration) were not related to the solar simulator results in any obvious way. Overall, phototoxicity from exposure to the sun was not a serious problem with HPPH (21). The observed phototoxicity from this solar simulator test and from the exposure of these patients to normal sunlight after their HPPH treatment was minimal. This can be contrasted with the phototoxicity from treatment with Photofrin, which induces cutaneous phototoxicity for a minimum of 3 weeks to several months (the usual

Table 2 *Skin response[a] in patients exposed to solar simulator light at various times after infusion with HPPH*

Patient no.	HPPH dose (mg/m^2)	HPPH AUC ($\mu g/ml \cdot h$)	24 h predicted HPPH plasma concentration ($\mu g/ml$)	Greatest skin response for various intervals between end of HPPH infusion and solar simulator test[b]				
				Preinfusion	24 h	48 h	72 h	Other
1	3	69.8	0.372	+	0	0		
2	3	55.2	0.362	0	+	+	+	
3	4	61.0	0.554	0	0	0	0	
4	4	102	0.685	0	0			
5	4	68.3	0.511	+	++		++	
6	4	105	0.736	0	++		0	
7	4	91.8	0.505	+	++			
8	4	265	0.302	0	0			
9	5	123	0.489	0	+	0		0[c]
10	5	62.3	0.751	0	0			
11	5	111	0.543	0		+		
12	6	223	0.474	++	++		+	
13	6	387	1.34	0	+++			
14	6	682	0.893	0	0			
15	6	147	0.721	0	+	0		
16	6	740	0.796	0	0			
17	6	90.8	0.477	0	+++	+++	+++	+++[d]
18	6	80.6	0.734	0	+++	++	0	
19	6	467	0.442	0	++	++	0	

[a] Response score: 0, no reaction; +, minimal perceptible erythema, blotchy areas of faint erythema confined to the illuminated site; ++, minimal erythema with sharp borders; +++, more pronounced erythema without edema; ++++, marked erythema with edema; +++++, marked erythema with edema and vesiculation.

[b] Solar simulator = 350–2500 nm light in a spectrum similar in shape to the sun and is equivalent to the exposure on a south-facing surface at an angle of 37° to the horizontal. This is the average irradiance for the continental United States. Fluence rate = 74 mW/cm^2. For each test, four separate skin spots were exposed to light for 10, 15, 20, or 30 min; the result in the table is the strongest skin response recorded for one test.

[c] Solar simulator light was applied 30 days after HPPH injection.

[d] Solar simulator light was applied 4 days after HPPH injection.

length of required eye and skin protection from bright light is 4–6 weeks, in our experience).

Examination of patient sera isolated up to 4 days after HPPH infusion showed no circulating metabolites. In addition, the incubation of HPPH with pooled human microsomes did not produce either phase I or II metabolites. For both assays, only HPPH and the few minor by-products (<3%) already present in the injectable preparation appeared on the reverse phase HPLC chromatographs (data not shown). Studies of other synthetic tetrapyrrolic photodynamic sensitizers (22–24) that also do not contain coordinated metal ions suggest that these compounds may not be easily metabolized *in vivo*. A comprehensive study, by us, of [^{14}C]HPPH in the tissues, plasma, feces, and urine of rats is planned.

Because this pharmacokinetic study includes patients with different diseases, different possible outcomes, different HPPH doses, and different light exposures, it would not be practical in this study to try to examine the relationship of HPPH pharmacokinetics to patient response. This type of pharmacodynamic analysis will become practical in future Phase II and Phase III studies of patients with the same disease.

A comprehensive population pharmacokinetic study and, if possible, a comprehensive population pharmacokinetic/pharmacodynamic study of an agent that is being introduced into clinical practice can often increase the utility of the new agent in routine clinical use (25). For the new photodynamic agent HPPH, the pharmacokinetic/pharmacodynamic study reported here will aid in the prediction of individual and population pharmacokinetic profiles. The unexplained variation in both profiles and physiological population parameters is acceptable. The increase of systemic clearance with age is a noteworthy finding and suggests that an upward dose adjustment may be useful for some elderly patients.

ACKNOWLEDGMENTS

We thank Dr. Patrick Smith (State University of New York at Buffalo School of Pharmacy and Pharmaceutical Sciences) for review of the project and suggestions in interpreting the pharmacokinetics of HPPH. We thank Drs. Barbara W. Henderson and Sandra O. Gollnick for critical reviews and comments, and we thank Barbara Owczarczak for technical support.

APPENDIX

Eq. 1 is a two-compartment biexponential pharmacokinetic model for the case of continuous infusion administration of drug. Eq. 1 was adapted from the standard equation for a two-compartment model with immediate bolus injection (12) by the method of Loo and Riegelman (13) to account for the effect of the 1-h infusion. All symbols are defined in Table 3 at the end of the Appendix. Eq. 1 is the structural pharmacokinetic model that was fit to the plasma-concentration-time raw data for each individual patient with SAS NLIN (14), with the direct estimation of four parameters for each patient: A, B, $t_{1/2\alpha}$, and $t_{1/2\beta}$.

$$C_P = \frac{At_{1/2\alpha}\left[1 - e^{-\frac{\ln(2)(t-t^*)}{t_{1/2\alpha}}}\right]e^{-\frac{\ln(2)t^*}{t_{1/2\alpha}}}}{\ln(2)\tau} + \frac{Bt_{1/2\beta}\left[1 - e^{-\frac{\ln(2)(t-t^*)}{t_{1/2\beta}}}\right]e^{-\frac{\ln(2)t^*}{t_{1/2\beta}}}}{\ln(2)\tau} \quad (1)$$

Eqs. 2 and 3 are useful intermediate equations, which are used with Eqs. 4–7, for the calculation of the four physiological pharmacokinetic parameters, plasma clearance (CL), distributional clearance (CL_D), volume of distribution of the central compartment (V_C), and volume of distribution at steady state (V_{SS}), from the four estimated empirical parameters, A, B, $t_{1/2\alpha}$, and $t_{1/2\beta}$ (12). Essentially, Eqs. 2–7 map the set of four empirical pharmacokinetic parameters to the set of four physiological pharmacokinetic parameters.

$$\mathrm{AUC} = \frac{\mathrm{A}}{\alpha} + \frac{\mathrm{B}}{\beta} \quad (2)$$

$$\mathrm{MRT} = \frac{\frac{\mathrm{A}}{\alpha^2} + \frac{\mathrm{B}}{\beta^2}}{\mathrm{AUC}} \quad (3)$$

$$\mathrm{CL} = \frac{\mathrm{D}}{\mathrm{AUC}} \quad (4)$$

$$\mathrm{CL_D} = \mathrm{D}\left[\frac{\alpha\mathrm{A} + \beta\mathrm{B}}{(\mathrm{A} + \mathrm{B})^2} - \frac{1}{\mathrm{AUC}}\right] \quad (5)$$

$$V_C = \frac{D}{A + B} \quad (6)$$

$$V_{SS} = (CL)(MRT) \quad (7)$$

Eqs. 8–15 perform the reverse mapping of the set of physiological pharmacokinetic parameters to the set of four empirical pharmacokinetic parameters. The use of Eqs. 8–15, along with Eq. 1, allow the direct estimation of the four physiological parameters, with nonlinear regression.

$$b = \frac{CL_D + CL}{V_C} + \frac{CL_D}{V_{SS} - V_C} \quad (8)$$

$$c = \frac{CL_D CL}{V_C(V_{SS} - V_C)} \quad (9)$$

$$\beta = \frac{b - \sqrt{b^2 - 4c}}{2} \quad (10)$$

$$\alpha = \frac{b + \sqrt{b^2 - 4c}}{2} \quad (11)$$

$$A = \frac{D\left(\frac{CL_D + CL}{V_C^2} - \frac{\beta}{V_C}\right)}{\alpha - \beta} \quad (12)$$

$$B = \frac{D\left(-\frac{CL_D + CL}{V_C^2} + \frac{\alpha}{V_C}\right)}{\alpha - \beta} \quad (13)$$

$$t_{1/2\alpha} = \frac{\ln(2)}{\alpha} \quad (14)$$

$$t_{1/2\beta} = \frac{\ln(2)}{\beta} \quad (15)$$

When using nonlinear mixed effects modeling, it is usually advantageous to scale the parameters that are directly estimated, so that all of the estimated parameters are of roughly the same magnitude (15). This was done in Eqs. 16–19. In addition, transformations can be applied to parameters to make the statistical assumption of a normal distribution for each parameter among patients more reasonable. This was done for V_{SS} in Eq. 17; a logarithmic transformation was applied, so that $\ln(V_{SS})$ is the actual parameter that is estimated. One can introduce additional covariates into the model that can potentially explain and thus reduce the patient to patient variance in parameters. This was done for CL in Eq. 18; the covariate, age (years) was introduced. The structural parameters that are actually directly estimated in Eqs. 16–20 are β_1, β_2, β_3, and β_4. Many parameters will vary from patient to patient, such as the four physiological pharmacokinetic parameters, CL, CL_D, V_C, and V_{SS}. One can introduce a random parameter for each structural pharmacokinetic parameter to quantify the spread of values of the pharmacokinetic parameters among patients. These random parameters are b_1, b_2, b_3, and b_4 in Eqs. 16–19. As is usual, it was assumed that the population mean for each of b_1, b_2, b_3, and b_4 is zero, and estimation was attempted for only the population variances and covariances for the set of four random variables. It was further assumed that each of these random variables was normally distributed. Note that in Table 1, the appropriate reverse parameter transformations were applied, and that the reported parameter estimates are for the physiological parameters, CL, CL_D, V_C, and V_{SS}; the four β and four b parameters are not listed.

$$V_C = 3.0\beta_1 + b_1 \quad (16)$$

$$V_{SS} = \exp(\beta_2 + b_2) \quad (17)$$

$$CL = \frac{\beta_3(age - 30.0)}{1200.0} + b_3 \quad (18)$$

$$CL_D = \frac{\beta_4}{10.0} + b_4 \quad (19)$$

The error variance model used for this study is Eq. 20. It was assumed that errors were normally distributed with a population mean of zero. Contributions to the total error come from both assay error and model misspecification error. This is a relative error model, and the square root of ϕ_2 is the overall coefficient of variation for the data.

$$\sigma^2_{error} = \phi_2[\text{true } C_P]^2 \quad (20)$$

To apply NLMIXED to the raw data, the above equations were coded into the SAS procedure language in the following order: Eqs. 16–19, 8–15, 1, and 20. This set of 14 equations was fit with SAS NLMIXED (15) using nonlinear mixed effects modeling to the entire data set for all 25 patients simultaneously.

The SAS code for the final run of the complete model will be emailed to any interested persons upon request.[5]

Table 3 *Definition of symbols*

Symbol or expression	Definition
D	Dose of HPPH given to patient (mg/m^2)
C_P	Concentration of HPPH measured in plasma (μg/ml)
τ	Infusion time (h)
t	Time from beginning of infusion (h)
t^*	0 during the infusion; t-τ after the end of the infusion (h)
A, B	Empirical parameters (μg/ml)
α	Rate constant for first exponential term (h^{-1})
β	Rate constant for second exponential term (h^{-1})
$t_{1/2\alpha}$	Half-life for first exponential term (h)
$t_{1/2\beta}$	Half-life for second exponential term (h)
MRT	Mean residence time (h)
AUC	Area under concentration-time curve from 0 to infinite time (μg/ml h)
CL	Plasma clearance (liter h^{-1}) or (liter m^{-2} h^{-1})
CL_D	Distributional clearance (liter h^{-1}) or (liter m^{-2} h^{-1})
V_C	Volume of distribution of central compartment (liter) or (liter/m^2)
V_{SS}	Volume of distribution at steady state (liter) or (liter/m^2)
b, c	Intermediate variables in Eqs. 8 and 9 used to simplify Eqs. 10 and 11
β_1, β_2, β_3, β_4	Structural parameters directly estimated with NLMIXED
b_1, b_2, b_3, b_4	Random parameters, normally distributed, for which the variances and covariances could be estimated with NLMIXED
σ^2_{error}	Error variance for normally distributed errors
ϕ_2	Error variance parameter; square root equivalent to coefficient of variation

REFERENCES

1. Dougherty, T. J. An update on photodynamic therapy applications. J. Clin. Laser Med. Surg., *20:* 3–7, 2002.
2. Dougherty, T. J., Gomer, C. J., Henderson, B. W., Jori, G., Kessel, D., Korbelik, M., *et al.* Photodynamic therapy. J. Natl. Cancer Inst. (Bethesda), *90:* 889–905, 1998.
3. Lee, L. K., Whitehurst, C., Pantelides, M. L., and Moore, J. V. *In situ* comparison of 665 nm and 633 nm wavelength light penetration in the human prostate gland. Photochem. Photobiol., *62:* 882–886, 1995.
4. Moriwaki, S. I., Misawa, J., Yoshinari, Y., Yamada, I., Takigawa, M., and Tokura, Y. Analysis of photosensitivity in Japanese cancer-bearing patients receiving photodynamic therapy with porfimer sodium (Photofrin). Photoderm. Photoimmunol. Photomed., *17:* 241–243, 2001.
5. Kessel, D., and Dougherty, T. J. Agents used in photodynamic therapy. Rev. Contemp. Pharmacother., *10:* 19–24, 1999.
6. Pandey, R. K., Bellnier, D. A., Smith, K. M., and Dougherty, T. J. Chlorin and porphyrin derivatives as potential photosensitizers in photodynamic therapy. Photochem. Photobiol., *53:* 65–72, 1991.
7. Henderson, B. W., Bellnier, D. A., Greco, W. R., Sharma, A., Pandey, R. K., Vaughan, L. A., *et al.* An *in vivo* quantitative structure-activity relationship for a congeneric series of pyropheophorbide derivatives as photosensitizers for photodynamic therapy. Cancer Res., *57:* 4000–4007, 1997.
8. Payne, J. T., McCaw, D. L., Casteel, S. W., Frazier, D., Rogers, K., and Tompson, R. V. Pharmacokinetics of pyropheophorbide-a-hexyl ether in the dog. Lasers Surg. Med., *18:* 406–409, 1996.
9. Bellnier, D. A., Henderson, B. W., Pandey, R. K., Potter, W. R., and Dougherty, T. J. Murine pharmacokinetics and antitumor efficacy of the photodynamic sensitizer 2-[1-hexyloxyethyl]-2-devinyl pyropheophorbide-a. J. Photochem. Photobiol. B Biol., *20:* 55–61, 1993.

10. Bellnier, D. A., Greco, W. R., Parsons, J. C., Oseroff, A. R., Kuebler, A., and Dougherty, T. J. An assay for the quantitation of Photofrin in tissues and fluids. Photochem. Photobiol., *66:* 237–244, 1997.
11. Woodburn, K., and Kessel, D. Effect of density-gradients on the binding of photosensitizing agents to plasma proteins. Int. J. Biochem. Cell Biol., *27:* 499–506, 1995.
12. Jusko, W. J. Guidelines for collection and analysis of pharmacokinetic data. *In:* W. E. Evans, J. J. Schentag, and W. J. Jusko, (eds.), Applied Pharmacokinetics, 3rd ed., pp. 2-1–2-43. Vancouver, WA: Applied Therapeutics Inc., 1992.
13. Loo, T. L., and Riegelman, S. Assessment of pharmacokinetic constants from post infusion blood curves obtained after IV infusion. J. Pharm. Sci., *59:* 53–55, 1970.
14. SAS Institute Inc. The NLIN Procedure. *In:* SAS/STAT User's Guide, Version 8, Vol. 2, pp. 2371–2418. Cary, NC: SAS Institute Inc., 1999.
15. SAS Institute Inc. The NLMIXED Procedure. *In:* SAS/STAT User's Guide, Version 8, Vol. 2, pp. 2419–2504. Cary, NC: SAS Institute Inc., 1999.
16. Pandey, R. K., Sumlin, A. B., Constantine, S., Aoudia, M., Potter, W. R., Bellnier, D. A., *et al.* Alkyl ether analogs of chlorophyll-a derivatives. I. Synthesis, photophysical properties and photodynamic efficacy. Photochem. Photobiol., *64:* 194–204, 1996.
17. Bellnier, D. A., and Dougherty, T. J. A preliminary pharmacokinetic study of intravenous Photofrin in patients. J. Clin. Laser Med. Surg., *14:* 311–314, 1996.
18. Freireich, E. J., Gehan, E. A., Rall, D. P., Schmidt, L. H., and Skipper, H. E. Quantitative comparison of toxicity of anticancer agents in mouse, rat, hamster, dog, monkey, and man. Cancer Chemother. Rep., *50:* 219–244, 1966.
19. Gibaldi, M., and McNamara, P. J. Apparent volumes of distribution and drug binding to plasma proteins and tissues. Eur. J. Clin. Pharmacol., *13:* 373–378, 1978.
20. MacKichan, J. J. Influence of protein binding and use of unbound (free) drug concentrations. *In:* W. E. Evans, J. J. Schentag, and W. J. Jusko (eds.), Applied Pharmacokinetics. 3rd ed., pp. 5-1–5-48. Vancouver, WA: Applied Therapeutics Inc., 1992.
21. Dougherty, T. J., Pandey, R. K., Nava, H. R., Smith, J. A., Douglass, H. O., Edge, S. B., *et al.* Preliminary clinical data on a new photodynamic therapy photosensitizer, 2-[1-hexyloxyethyl]-2-devinylpyropheophorbide-a (HPPH), for treatment of obstructive esophageal cancer. *In:* T. J. Dougherty (ed.), Optical Methods for Tumor Treatment and Detection: Mechanisms and Techniques in Photodynamic Therapy, Vol. 3909, pp. 25–27. Bellingham, WA: SPIE Press, 2000.
22. Tomio, L., Zorat, P. L., Jori, G., Reddi, E., Salvato, C., *et al.* Elimination pathway of hematoporphyrin from normal and tumor-bearing rats. Tumori, *68:* 283–286, 1982.
23. Cai, H., Wang, Q., Luo, J., and Lim, C. K. Study of temoporfin metabolism by HPLC and electrospray mass spectrometry. Biomed. Chromatogr., *13:* 354–359, 1999.
24. Bellnier, D. A., Ho, Y-K., Pandey, R. K., Missert, J. R., and Dougherty, T. J. Distribution and elimination of Photofrin II in mice. Photochem. Photobiol., *50:* 221–228, 1989.
25. United States Department of HHS, FDA, CDER, CBER. Guidance for Industry Population Pharmacokinetics. pp. 1–31. Rockville, MD; Office of Training and Communications, Division of Communications Management, 1999.